ACS OMEGA

http://pubs.acs.org/journal/acsodf

Article

Carbon Dot-Modified Branched TiO_2 Photoelectrochemical Glucose Sensors with Visible Light Response

Run Yuan, Bingdong Yan, Caiyan Lai, Xiaohong Wang, Yang Cao, Jinchun Tu, Yi Li,* and Qiang Wu*

Cite This: *ACS Omega* 2023, 8, 22099−22107

Read Online

ACCESS | Metrics & More | Article Recommendations | Supporting Information

ABSTRACT: The development of a photoelectrochemical (PEC) sensor for the sensitive and rapid detection of glucose is highly desirable. In PEC enzyme sensors, inhibition of the charge recombination of electrode materials is an efficient technique, and detection in visible light can prevent enzyme inactivation due to ultraviolet irradiation. In this study, a visible light-driven PEC enzyme biosensor was proposed, using CDs/branched TiO_2 (B-TiO_2) as the photoactive material and glucose oxidase (GOx) as the identification element. The CDs/B-TiO_2 composites were produced via a facile hydrothermal method. Carbon dots (CDs) can not only act as photosensitizers but also inhibit photogenerated electron and hole recombination of B-TiO_2. Under visible light, electrons in the carbon dots flowed to B-TiO_2 and further to the counter electrode through the external circuit. In the presence of glucose and dissolved oxygen, H_2O_2 generated through the catalysis of GOx could consume electrons in B-TiO_2, causing a decrease in photocurrent intensity. Ascorbic acid was added to ensure the stability of the CDs during the test. Based on the variation of the photocurrent response, the CDs/B-TiO_2/GOx biosensor presented a good sensing performance of glucose in visible light, its detection range was from 0 to 9.00 mM, and the detection limit was 0.0430 mM.

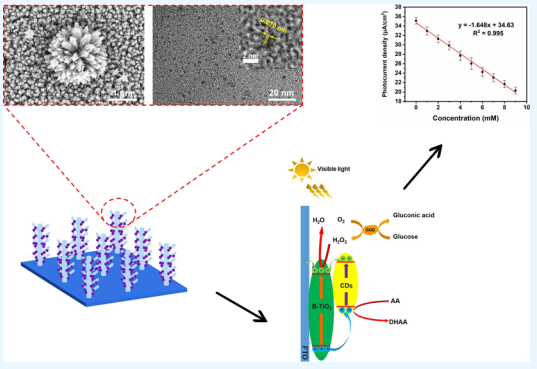

1. INTRODUCTION

Blood glucose levels in the body are associated with life and health, and abnormal blood glucose levels usually result in numerous diseases, such as hypoglycemia and diabetes.[1] This situation means that there is an urgent need for a fast and convenient method of glucose detection. In recent years, numerous common analytical techniques have been applied to the glucose detection, such as fluorescence, colorimetry, electrochemical, and photoelectrochemical (PEC) analysis.[2,3] Among them, PEC measurement techniques have been extensively utilized in biological testing and detection because their sensors are easy to transport, simple to operate, can respond quickly, and are highly sensitive.[4]

TiO_2 nanorods (NRs) have been widely used for PEC sensors owing to their high photocorrosion resistance, good chemical stability, nontoxicity to the humans, and low preparation cost.[5,6] Dendritic TiO_2 is a type of TiO_2 with nanobranches growing around the trunk, and it is also named branched TiO_2 (B-TiO_2).[7,8] This type of titanium dioxide is considered as a potential photoactive material for the development of high-sensitivity PEC sensors based on its outstanding light-harvesting features and highly conductive channel for charge carrier collection.[9,10] However, as a wide band gap semiconductor, TiO_2 is usually active only under ultraviolet radiation, which not only prevents it from effectively using the full energy of the sun but also causes biological samples to be vulnerably destructed under ultraviolet light.[11] Numerous techniques, including dye sensitization, element doping, and combination with narrow band gap semiconductors, have been investigated to expand the excitation source of TiO_2 into the visible range and subsequently solve the aforementioned issues while enhancing the performance of PEC sensors.[12]

CDs are an emerging zero-dimensional material that features a small size, high water solubility, low toxicity, and good biocompatibility.[13,14] TiO_2 with excellent PEC properties modified by CDs has been highly appreciated by researchers. For instance, Bian et al.[15] coupled CDs to TiO_2, and the CDs could collect electrons and help adsorb dichromate ions, resulting in CDs/TiO_2 that were 5.40 times more active than pure TiO_2 in the photoreduction of Cr(VI). Ke et al. coupled TiO_2 nanospheres with upconverted CDs by using a sol−gel procedure, and the composite exhibited excellent photodegradation of methylene blue even when exposed to visible light.[16] The good conductivity of CDs contributes to charge separation and transfer. Zhu et al. modified CDs to binary TiO_2−Cu composites; the CDs acted as an electron mediator in the multistep electron transfer, allowing TiO_2−Cu activity to be

Received: April 2, 2023
Accepted: May 17, 2023
Published: June 5, 2023

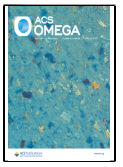

https://doi.org/10.1021/acsomega.3c02202
ACS Omega 2023, 8, 22099−22107

Scheme 1. Flowchart for the Fabrication of CDs/B-TiO_2

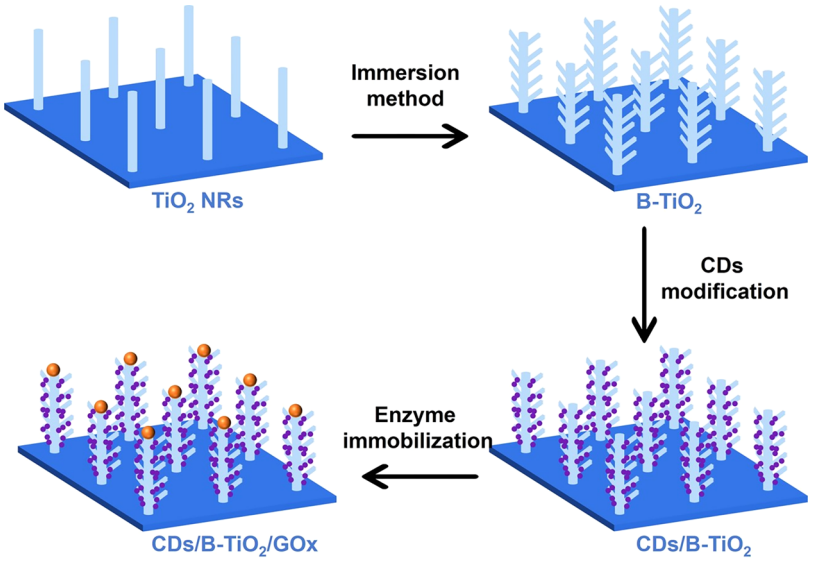

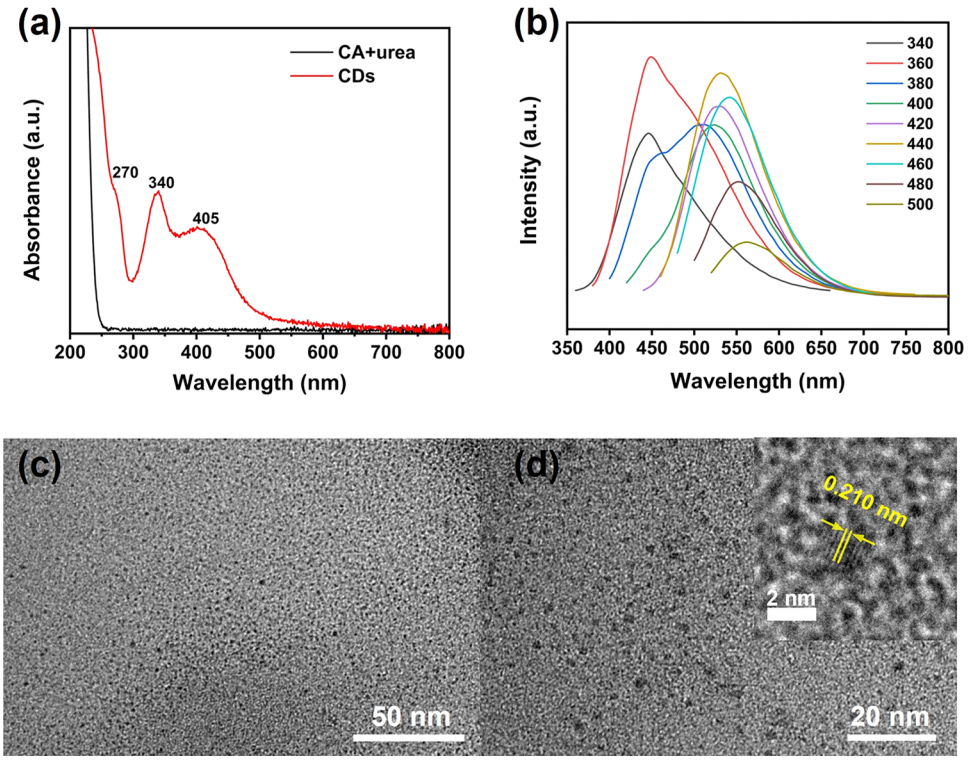

Figure 1. (a) UV−vis absorption spectroscopy of CDs, CA, and urea in aqueous solution; (b) PL diagram of the CD solution excited at wavelengths from 340 to 500 nm; and (c, d) TEM images of CDs at different magnifications.

further boosted.[17] However, the stability of CDs under test conditions remains a problem.

A glucose oxidase (GOx) biosensor based on CD-sensitized B-TiO_2 that could detect glucose under visible light was developed in this work. Three-dimensional structured TiO_2 was constructed by growing ultrathin nanosheets on the surface of nanorods in a two-step process. The CDs were synthesized in a simple and low-cost manner by taking citric acid (CA) and urea as original materials. The obtained specimens presented numerous hydrophilic functional groups (e.g., amino, carboxyl, and hydroxyl groups, among others) to the extent that they could provide greater biocompatibility for subsequent immobilization of GOx. After the addition of CDs, the light collection ability of TiO_2 to visible light was significantly enhanced. In addition, a certain amount of ascorbic acid (AA) was added as a hole sacrificial agent to ensure the stability of the CDs during the test.[18] The PEC sensor could operate in visible light, avoiding enzyme inactivation due to ultraviolet exposure. The CDs/B-TiO_2/GOx sensor showed reliable glucose detection under visible light.

2. EXPERIMENTAL METHODS

2.1. Synthesis of Rutile TiO_2 NRs. TiO_2 NRs were constructed via hydrothermal in-growth on FTO substrates

https://doi.org/10.1021/acsomega.3c02202
ACS Omega 2023, 8, 22099−22107

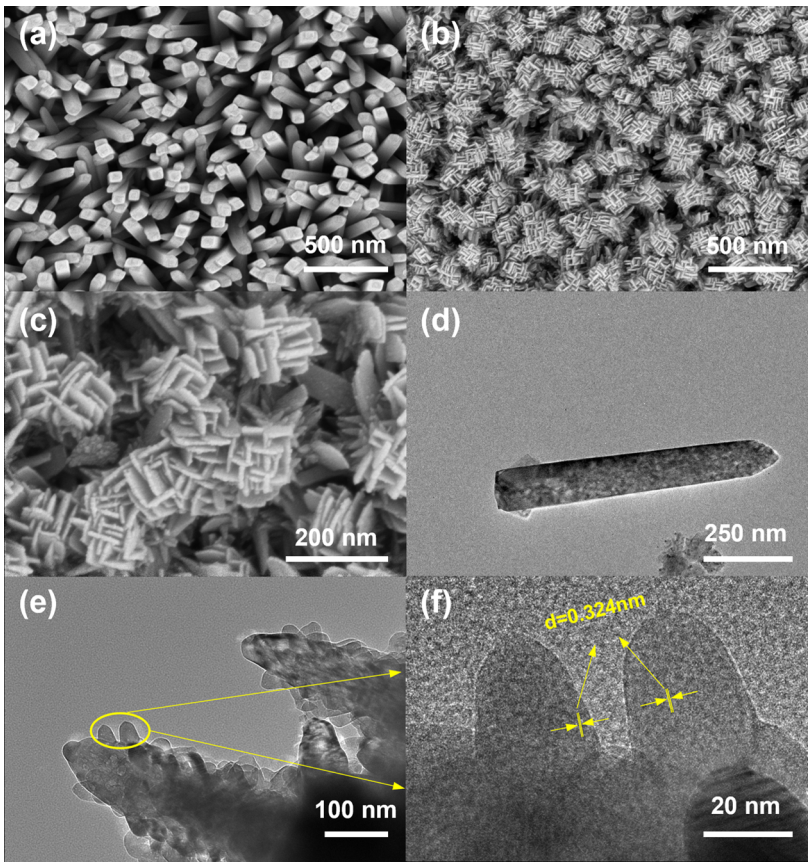

Figure 2. (a) SEM of rutile TiO_2 NRs, (b, c) SEM of B-TiO_2, (d) TEM of rutile TiO_2 NRs, (e) TEM of B-TiO_2, and (f) HRTEM of B-TiO_2.

(Scheme 1).[19] First, FTO glass substrates were cleaned with a glass cleaning reagent in an ultrasonic instrument for 20.0 min and rinsed with ultrapure water. Second, 10.0 mL of deionized water was mixed with 10.0 mL of HCI by stirring for 10.0 min, and 0.400 mL of tetrabutyl titanate was added dropwise to this solution and stirred for half an hour. The solution was then poured into a 50.0 mL Teflon container, and two FTO glasses were positioned into the abovementioned solution with their conductive surfaces facing down. The hydrothermal reaction was performed at 150 °C for 4.00 h. The FTO substrates were flushed with water after natural cooling. Finally, annealing was performed in a constant-temperature resistance furnace at 500 °C for 3.00 h to enhance the crystallinity of the material.

2.2. Synthesis of B-TiO_2. B-TiO_2 samples based on the TiO_2 NRs were prepared via the immersion method.[20] Briefly, 20.0 mL of deionized water was mixed with 0.250 mL of HCl, and then 0.250 mL of $TiCl_3$ was added dropwise and stirred for half an hour to form a homogeneous solution. The two TiO_2 NR samples were positioned into the abovementioned solution with their conductive surfaces facing down and then placed in an oven and kept at 80.0 °C for 1.00 h. The products were flushed with water after natural cooling. Finally, an annealing process was performed in a constant-temperature resistance furnace at 500 °C for 3.00 h to enhance the crystallinity of the material.

2.3. Fabrication of CDs/B-TiO_2. A simple and low-cost method to synthesize CDs was used in this study.[21] Briefly, 1.00 g of CA and 1.00 g of urea were decanted into 10.0 mL of water and stirred until the materials were completely dissolved. The aforementioned solution was then reacted in an 800 W commercial microwave oven for approximately 3.00 min. The clear solution gradually turned yellow and then brown. When the water eventually evaporated, black solids formed. The resulting CDs were dissolved in water and placed in a centrifuge at 12,000 rpm for 30.0 min to remove suspended impurities and subsequently obtain the CD solution. CDs/B-TiO_2 could also be obtained by placing B-TiO_2 into the solution and heating it to 80.0 °C for 12.0 h.

2.4. Fabrication of CDs/B-TiO_2/GOx. 10.0 μL of GOx solution and 10.0 μL of chitosan solution were dropped onto the CDs/B-TiO_2 composites, and then CDs/B-TiO_2/GOx were placed in the upper layer of the refrigerator for standby.

3. RESULTS AND DISCUSSION

3.1. Characterizations of CDs, TiO_2 NRs, B-TiO_2, and CDs/B-TiO_2. The aqueous solution of CA and urea as raw materials had no absorption in the visible light region, which contrasts with the solution after microwave treatment. (Figure 1a). The CD solution had a wide absorption spectrum, with peaks mainly appearing at 270, 340, and 405 nm, which are mainly aromatic conjugated absorption peaks. Figure 1b illustrates the CD excitation-dependent emission with an excitation wavelength of 340−500 nm. With increasing excitation wavelength, the emission wavelength gradually moved toward a higher frequency. This excitation-dependent emission may be the result of surface and size inconsistencies in the CDs.[22] Figure S1 shows the X-ray diffractometry of powder CDs. An extremely wide diffraction peak appears at approximately $2\theta = 26°$, which is close to the diffraction peak of the graphite (002) crystal plane, just because the carbon atoms in the CDs were highly disordered.[23] Figure 1c,d presents the TEM images of the CDs, which have a diameter between 1.00 and 3.00

https://doi.org/10.1021/acsomega.3c02202
ACS Omega 2023, 8, 22099−22107

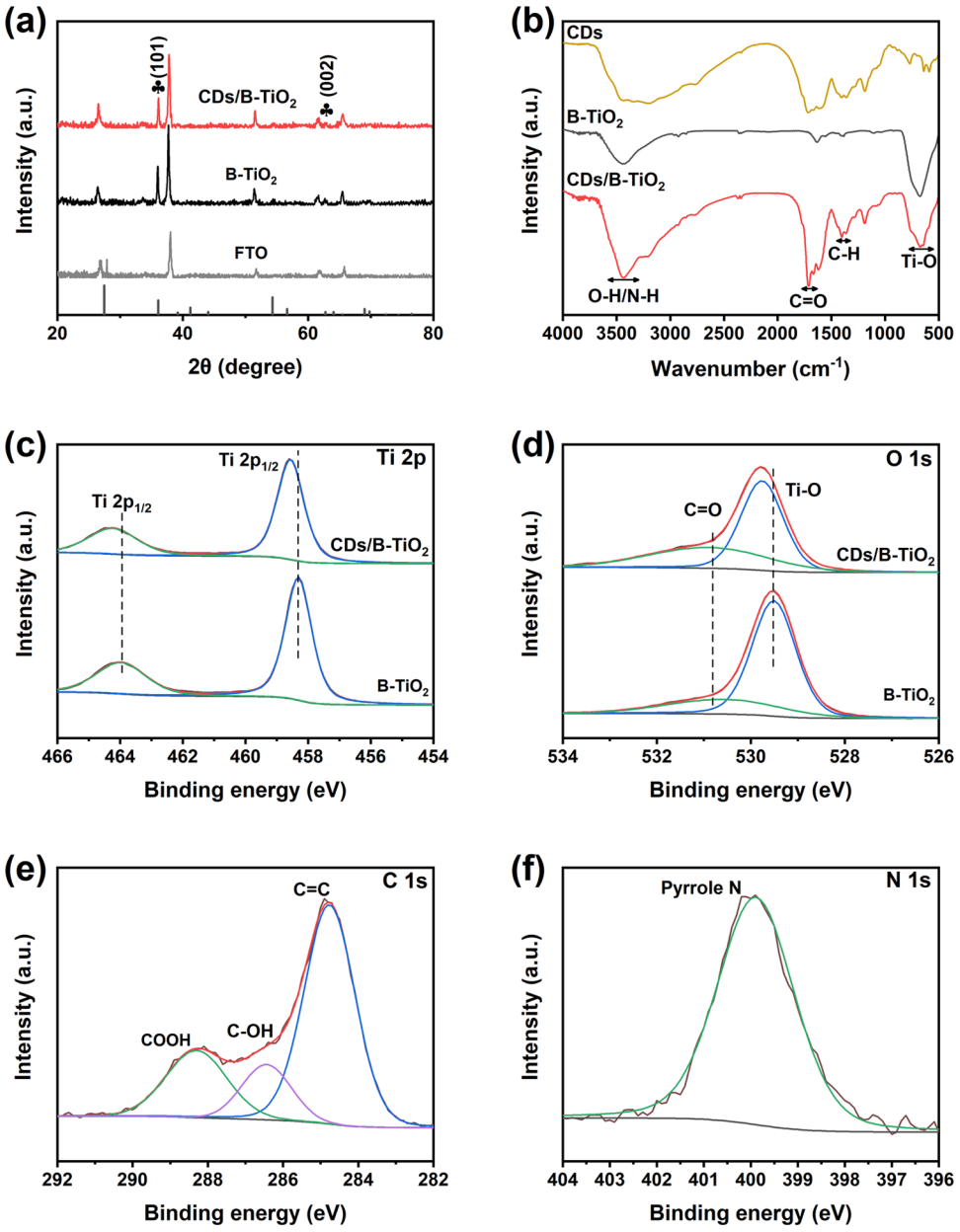

Figure 3. (a) XRD spectra of FTO, B-TiO_2, and CDs/B-TiO_2; (b) FTIR spectra of CDs, B-TiO_2, and CDs/B-TiO_2 and high-resolution XPS of B-TiO_2 and CDs/B-TiO_2 samples, (c) Ti 2p, (d) O 1s, (e) C 1s, and (f) N 1s.

nm. A crystal plane spacing of 0.210 nm was also observed, which corresponds to the (100) facet of graphite.[22]

The morphologies of the rutile TiO_2 NRs and B-TiO_2 samples are shown in Figure 2. The vertical view of rutile TiO_2 NRs is presented in Figure 2a. The TiO_2 NRs were regularly fixed on FTO glasses, and they had a diameter of approximately 110 nm (Figure 2d). Figure 2b,c shows the uniform coating of the distinct ultrathin nanosheets on the entire wall of the TiO_2 NRs, which made TiO_2 have a three-dimensional hierarchical structure. More details about ultrathin nanosheets are shown in Figure 2e. Figure 2f shows the HRTEM image captured close to the edge of the TiO_2 NRs (marked in Figure 2e), in which branches grow on the surface of the nanorods and have good crystallinity; the lattice fringe of this branch is d = 0.324 nm, corresponding to the rutile (110) crystal plane.[24]

The XRD diagram of the CDs/B-TiO_2 composite is shown in Figure 3a. The two diffraction peaks appearing at 36.1 and 62.7° correspond to the (101) and (002) crystal planes of rutile TiO_2, respectively; these findings are in accord with the data reported in the PDF card (JCPDS No. 21-1276). Another peak at 2θ = 26.7, 37.9, 61.6, and 65.8° originates from the FTO substrate. The noncharacteristic diffractive peaks of CDs can be ascribed to the small proportion of CDs in the materials.[20] Then, FTIR spectroscopy was used to detect functional groups of the materials themselves and those that were adsorbed onto the materials (Figure 3b).[25] The broad absorption peak at 3300−3600 cm^{-1} corresponds to the stretching vibration peak of hydroxyl and amino groups. Absorption bands at 1600−1770 cm^{-1} were assigned to ν(C═O). The absorption band at 1350−1460 cm^{-1} corresponds to the in-plane bending vibration of the C−H bond.[21]

The XPS of CDs/B-TiO_2 (Figure 3) was used to analyze the components and related chemical bonds. Figure S2 shows the full spectra of the TiO_2 and CDs/B-TiO_2 samples. The spectrum

https://doi.org/10.1021/acsomega.3c02202
ACS Omega 2023, 8, 22099−22107

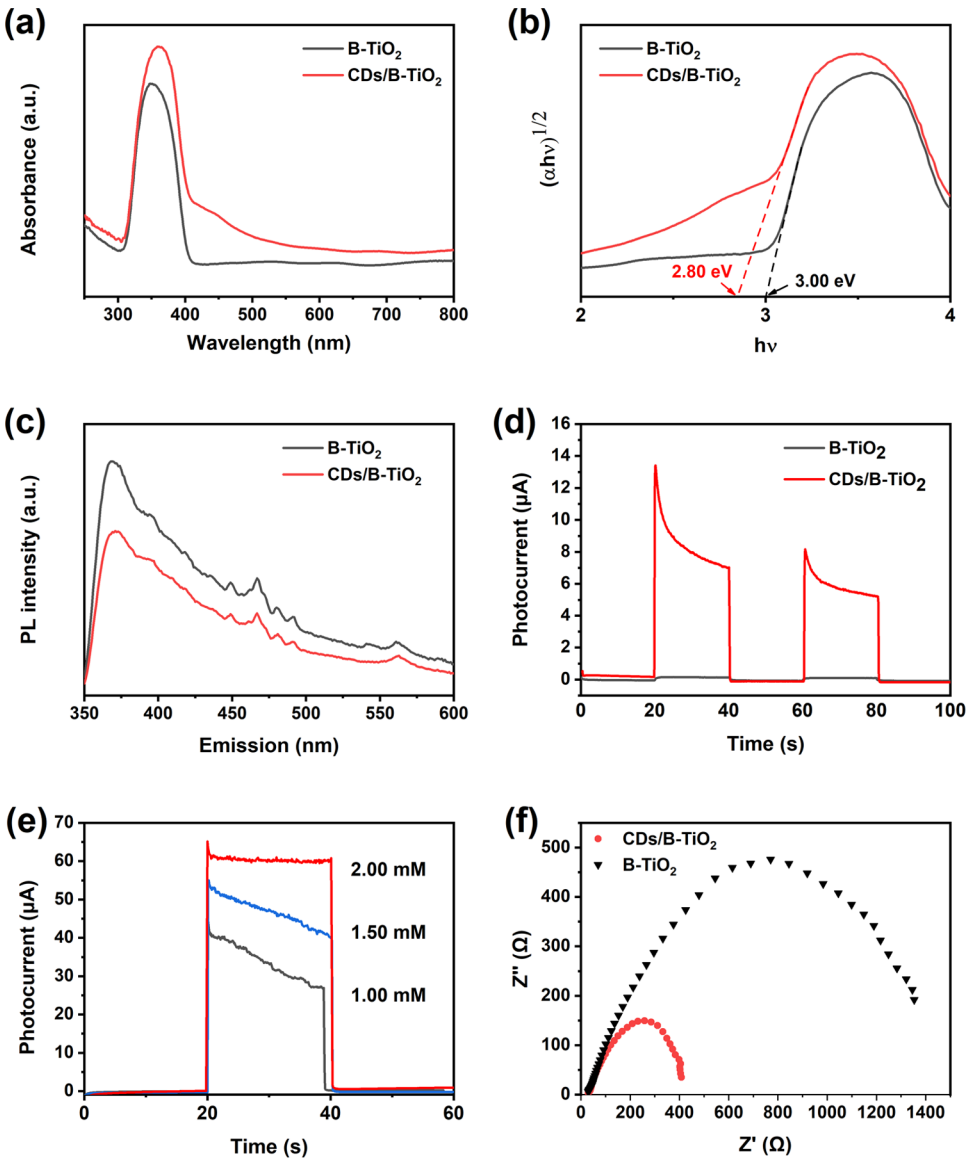

Figure 4. (a) UV−visible diffuse−reflection spectroscopy, (b) Tauc plots of B-TiO_2 and CDs/B-TiO_2, (c) PL of B-TiO_2 and CDs/B-TiO_2, (d) photocurrent response at 0 V, (e) photocurrent response at 1.00−2.00 mM ascorbic acid, and (f) EIS measurements.

of the CDs/B-TiO_2 sample highlights the four elements of C, N, O, and Ti. The new appearance of the N peak in CDs/B-TiO_2 can be attributed to the CDs, further indicating the successful combination of CDs and B-TiO_2. Two peaks at 464.0 and 458.3 eV were observed for Ti $2p_{1/2}$ and Ti $2p_{3/2}$, respectively, corresponding to the Ti(IV) ion in the titanium dioxide crystal (Figure 3c).[26,27] Similar Ti components were observed in CDs/B-TiO_2, but their binding energy slightly changed. As shown in Figure 3d, the peak at 530.6 eV is the result of the presence of C═O bonding, and the peak appearing at 529.5 eV can be explained by the presence of oxygen in the lattice. Similarly, the positions of these peaks shifted in the CDs/B-TiO_2 sample. Compared with the position of B-TiO_2, the position of Ti 2p and O 1s in the CDs/B-TiO_2 composites had a slight negative shift, indicating that the surface chemical environment of Ti and O in CDs/B-TiO_2 composites had changed due to the strong mutual influence between CDs and B-TiO_2.[28] The high-resolution C 1s XPS data (Figure 3e) were fitted by three peaks at 288.3, 286.3, and 284.7 eV for COOH, C−OH, and C═C, respectively.[29] Enriched with hydrophilic groups, the obtained CDs could be easily dispersed into water, allowing for the uniform decoration of CDs on the TiO_2 surface. What is more, in some papers, the combination of CDs including functional groups such as C−OH and COOH with TiO_2 is assisted by Ti−O−C bonds.[29−31] The N 1s spectrum showed only one peak at 399.9 eV, which can be ascribed to the pyrrole N (Figure 3f).[30]

3.2. PEC Characterizations of the CDs/B-TiO_2 Electrode. The optical absorbance intensity of the prepared electrode materials after exposure to visible light was evaluated on the basis of the recorded UV−vis spectra (Figure 4a) at wavenumbers ranging from 250 to 800 nm. B-TiO_2 had a lower absorption intensity between 400 and 800 nm compared with the optical absorbance intensity in the ultraviolet range, which can be explained by the inherent absorption characteristic of TiO_2.[13,14] After adding CDs to B-TiO_2, the ability of the material to capture light was enhanced not only in the ultraviolet range but also in the visible range. The results demonstrated the successful decoration of CDs and their contributions to improving light absorption performance. The band gaps could

https://doi.org/10.1021/acsomega.3c02202
ACS Omega 2023, 8, 22099−22107

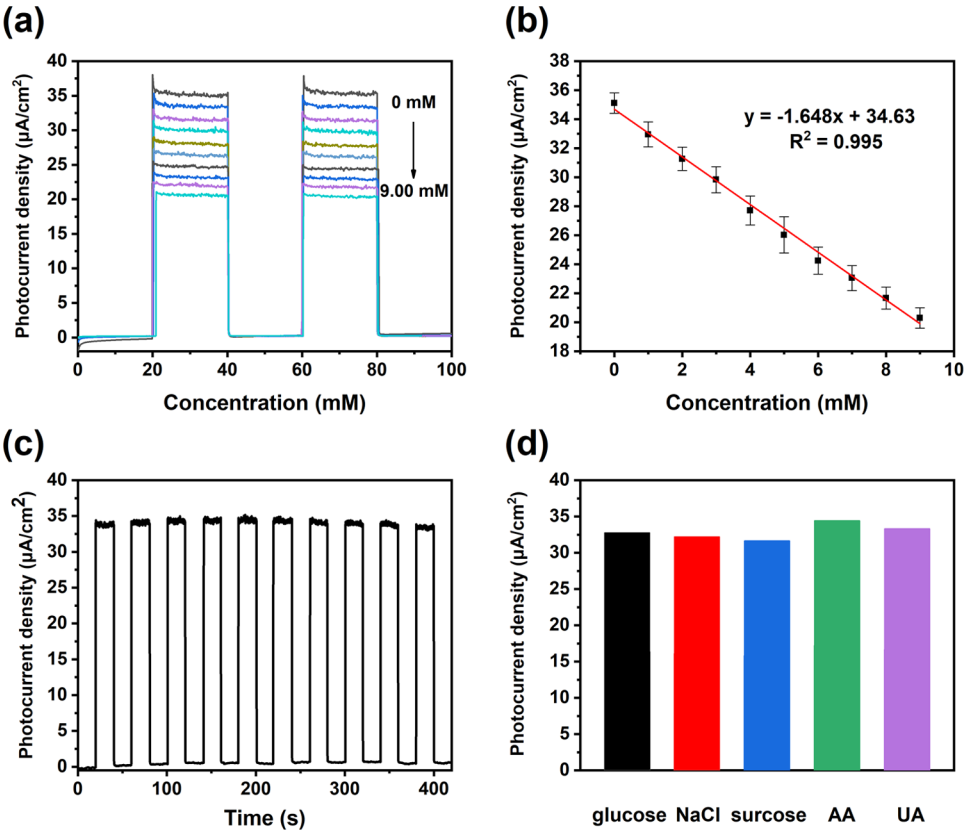

Figure 5. (a) Photocurrent density of CDs/B-TiO_2/GOx at 0 V in 0.100 M PBS (pH = 7.40), (b) linear calibration for the CDs/B-TiO_2/GOx biosensor in 0.100 M PBS (pH = 7.40), (c) stability test in the presence of 1.00 mM glucose, and (d) photocurrent density of CDs/B-TiO_2/GOx in 0.100 M PBS (pH = 7.40) with other substances: NaCl, Suc, AA, and UA.

be calculated using the Kubelka–Munk transformation[32,33] as follows

$$ahv = A(hv - Eg)^2$$

where α, h, v, and A represent the absorption coefficient, Planck's constant, light frequency, and proportionality constant, respectively. As shown in Figure 4b, the band gap energies of pristine B-TiO_2 and CDs/B-TiO_2 are 3.00 and 2.80 eV, respectively, which further confirms the absorptive capability of CD-modified B-TiO_2 to absorb more sunlight and utilize more solar energy to improve the PEC performance.

Figure 4c shows the PL spectra of B-TiO_2 and CDs/B-TiO_2 composites under excitation at 325 nm. The shape lines of the two samples were comparable. This finding indicates that the addition of CDs to TiO_2 causes no additional fluorescence, although it may influence the intensity of emission peaks. Compared with the findings for B-TiO_2, the photoluminescence intensity of CDs/B-TiO_2 was significantly reduced. The quenched PL emission reveals that the addition of CDs could produce an inhibitory effect on charge recombination in the pristine B-TiO_2 sample. In this case, the CDs in the composites acted as electron traps, subsequently capturing the photogenerated electrons from the B-TiO_2 and prolonging the existence of charge carriers by slowing down the recombination of photogenerated electron–hole pairs.[34] This finding agrees with the average lifetime results measured by time-resolved PL spectroscopy (Figure S3 and Table S1).

The PEC behaviors of CDs/B-TiO_2 and B-TiO_2 were further evaluated in this work. By using B-TiO_2 and CDs/B-TiO_2 electrodes as working electrodes, transient photocurrent measurements were performed under visible light at wavelengths of >420 nm (Figure 4d). The photocurrent response of B-TiO_2 was less than 1.00 μA, and the photocurrent response of CDs/B-TiO_2 reached approximately 10.0 μA with the addition of CDs. However, the CDs under the test conditions were not sufficiently stable. The photocurrent decreased within 20.0 s of light exposure, so AA was added to the PBS to ensure stability during testing. Figure 4e shows the photocurrent response after the addition of AA (from 1.00 to 2.00 mM). The photocurrent continuously decreased after adding 1.00 and 1.50 mM AA, but the photocurrent response stabilized around a certain value after adding 2.00 mM AA. Therefore, for the subsequent testing of glucose, the concentration of AA was chosen to be 2.00 mM.

Additionally, electrochemical impedance spectroscopy (EIS) was utilized to examine the efficiency of separation and transfer of photogenerated charges. The charge transfer resistance can be determined on the basis of the radius of a semicircle—a semicircle with a small radius represents a small resistance, further indicating an as-fabricated photoelectrode with a high-quality charge transfer.[35,36] As shown in Figure 4f, with respect to B-TiO_2, the semicircular radius of the CDs/B-TiO_2 hybrids was much smaller, indicating that the latter specimens have faster charge transfer characteristics, which can be attributed to the excellent electrical conductivity of the CDs.[37]

3.3. Characterization of the CDs/B-TiO_2/GOx Biosensor for Glucose. The sensing behavior of the PEC biosensor was investigated by detecting different concentrations of glucose under simulated sunlight (wavelengths of >420 nm). The relationship between the photocurrent density of the CDs/B-TiO_2/GOx electrode and glucose concentration was tested

https://doi.org/10.1021/acsomega.3c02202
ACS Omega 2023, 8, 22099−22107

under continuous stirring (Figure 5a). With the continuous addition of glucose, a substantial decrease in the photocurrent was observed. In other words, the intensity of the photocurrent decreased with increasing glucose concentration. The derived relationship between photocurrent intensity and glucose concentration indicates a solid linear association between the two variables. As shown in Figure 5b, the corresponding linearization equation is J (photocurrent density) (μA cm^{-2}) = −1.648 [Glu] (mM) + 34.63 (mM), and the correlation coefficient of statistical significance is 0.995. Thus, the sensitivity of the biosensor under simulated sunlight was 1.648 μA mM^{-1} cm^{-2}, with a detection range of 0−9.00 mM for glucose, and the detection limit (LOD) (S/N = 3.00) was 0.0430 mM.

The stability of the CDs/B-TiO_2/GOx electrode was tested at 1.00 mM glucose via intermittent exposure for 420 s (Figure 5c). After nine on/off cycles, the photocurrent response of the CDs/B-TiO_2/GOx electrode changed slightly, demonstrating the high stability of this sensor.

Specificity and selectivity are essential metrics for evaluating sensor performance.[38,39] Here, molecules that might appear in serum, such as NaCl, sucrose (Suc), AA, and UA, were employed as disruptors to test the performance of the CDs/B-TiO_2/GOx biosensor. In addition, the concentration of the added species in blood was 0.100 mM, which was one-tenth of the concentration of glucose. As shown in Figure 5d, the photocurrent density of the CDs/B-TiO_2/GOx biosensor did not change greatly after the addition of the aforementioned interfering species. This finding may be attributed to the selectivity of glucose oxidase fixed on the electrode surface, proving the good anti-interference property of the sensor (Table 1).

Table 1. Analytical Performance of Several GOx PEC Biosensors

PEC biosensors	dynamic range (mM)	detection limit (mM)	refs
α-Fe_2O_3	0.200−2.00	0.0150	40
GOx/CdTe	0.100−11.0	0.0400	41
GOx/Ag_2S/SnO_2	0.100−12.2	0.0320	42
ZnS/SG-GOx	0.100−5.50	0.0200	43
graphene-WO_3-Au/GOx	0.500−7.00	0.0150	44
ZnO/GOx/Nafion	0−10.0	N/A	45
MoS_2−TiO_2/GOx	0.100−10.0	0.0150	46
TiO_2/CdSe@CdS/GOx	1.00−10.0	N/A	47
CDs/B-TiO_2/GOx	**0−9.00**	**0.0430**	**this work**

3.4. Principle of the PEC Biosensor. After exposure to visible illumination, the electron−hole pairs of B-TiO_2 and CDs were generated (formula 1). Due to the higher conduction band position of CDs, photogenerated electrons excited within the CDs were injected into the B-TiO_2. And these electrons rapidly migrated to the FTO glass and then to the counter electrode through the external circuit so that the initial photocurrent was formed (formula 2).[45] Furthermore, CDs are excellent electron transport media that can transfer electrons and accept photogenerated holes from B-TiO_2. Thus, in this work, the photogenerated holes in TiO_2 were injected into the valence band of the CDs. The holes that migrated toward the CDs were consumed by AA in the electrolyte solution (formula 3), allowing the CDs to be properly protected. After adding glucose to the solution, dissolved oxygen and glucose were catalyzed by GOx to generate H_2O_2 and gluconic acid (formula 4). The generated H_2O_2 could react with the photogenerated electrons from the B-TiO_2 (formula 5). As the glucose concentration in the electrolytic cell increased, the continuously produced H_2O_2 further consumed photogenerated electrons, subsequently reducing the photocurrent (Scheme 2). Therefore, different glucose concentrations can produce different electrical signals. The reaction formula is as follows

Scheme 2. PEC Detection Mechanism of Glucose by CDs/B-TiO_2/GOx

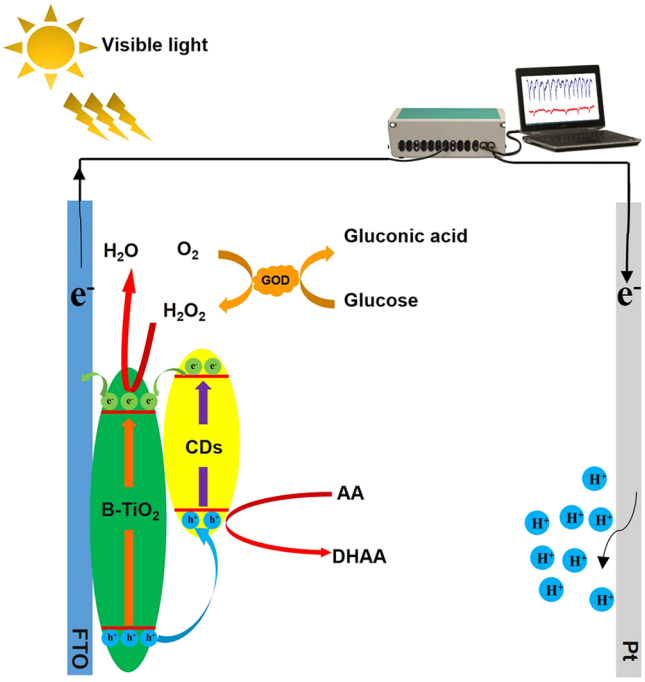

$$h\nu \rightarrow e^-_{CB} + h^+_{VB} \quad (1)$$

$$H^+ + e^- \rightarrow H_2 \quad (2)$$

$$h^+_{VB} + AA \rightarrow DHAA \quad (3)$$

$$O_2 + \text{glucose} \xrightarrow{GOx} H_2O_2 + \text{glucose acid} \quad (4)$$

$$H_2O_2 + e^-_{CB} \rightarrow H_2O \quad (5)$$

4. CONCLUSIONS

In summary, we have successfully designed a visible light-driven PEC enzyme biosensor for glucose detection based on CDs/B-TiO_2 composites, which was synthesized by a hydrothermal approach. CDs were grown on the surface of B-TiO_2 in situ, and good chemical bonding was the basis for the directional movement of charges between them. The CDs not only extended the light absorption range of B-TiO_2 and increased the intensity of visible light response but also enabled CDs/B-TiO_2 composites to have a longer photogenerated electron lifetime and faster carrier transport efficiency. Consequently, the acquired CDs/B-TiO_2/GOx PEC biosensor showed excellent stability and satisfactory reproducibility. The as-prepared CDs/B-TiO_2/GOx glucose biosensor obtained satisfactory results under simulated sunlight with a sensitivity of 1.648 μA mM^{-1} cm^{-1}, a linear detection range of 0−9.00 mM, and an LOD (S/N

https://doi.org/10.1021/acsomega.3c02202
ACS Omega 2023, 8, 22099−22107

= 3.00) of 0.0430 mM in PBS buffer at pH 7.40. The sensor works in visible light to reduce damage to biomolecules; thus, this design offers a viable route to the future development of economical, green, and practical glucose detection devices.

■ ASSOCIATED CONTENT

Supporting Information

The Supporting Information is available free of charge at https://pubs.acs.org/doi/10.1021/acsomega.3c02202.

Materials and reagents; characterization instruments; PEC test; XRD spectrum of CDs; XPS of B-TiO_2 and CDs/TiO_2 for full survey; time-resolved photoluminescence of B-TiO_2 and CDs/TiO_2; and lifetimes calculated by the exponential decay function of B-TiO_2 and CDs/TiO_2 (PDF)

■ AUTHOR INFORMATION

Corresponding Authors

Yi Li − *State Key Laboratory of Marine Resource Utilization in South China Sea, School of Materials Science and Engineering, Hainan University, Haikou 570228, P. R. China*; Email: liyi@hainanu.edu.cn

Qiang Wu − *The Second Affiliated Hospital, School of Tropical Medicine, Key Laboratory of Emergency and Trauma of Ministry of Education, Research Unit of Island Emergency Medicine, Chinese Academy of Medical Sciences (No. 2019RU013), Hainan Medical University, Haikou 571199, P. R. China*; orcid.org/0000-0003-3922-5189; Email: wuqiang001001@aliyun.com

Authors

Run Yuan − *State Key Laboratory of Marine Resource Utilization in South China Sea, School of Materials Science and Engineering, Hainan University, Haikou 570228, P. R. China*

Bingdong Yan − *State Key Laboratory of Marine Resource Utilization in South China Sea, School of Materials Science and Engineering, Hainan University, Haikou 570228, P. R. China*

Caiyan Lai − *State Key Laboratory of Marine Resource Utilization in South China Sea, School of Materials Science and Engineering, Hainan University, Haikou 570228, P. R. China*

Xiaohong Wang − *State Key Laboratory of Marine Resource Utilization in South China Sea, School of Materials Science and Engineering, Hainan University, Haikou 570228, P. R. China*

Yang Cao − *State Key Laboratory of Marine Resource Utilization in South China Sea, School of Materials Science and Engineering, Hainan University, Haikou 570228, P. R. China*

Jinchun Tu − *State Key Laboratory of Marine Resource Utilization in South China Sea, School of Materials Science and Engineering, Hainan University, Haikou 570228, P. R. China*; orcid.org/0000-0001-8793-4727

Complete contact information is available at: https://pubs.acs.org/10.1021/acsomega.3c02202

Notes

The authors declare no competing financial interest.

■ ACKNOWLEDGMENTS

This research was financially supported by the Hainan Province Science and Technology Special Fund (Nos. ZDKJ2021029, ZDYF2021SHFZ068), the National Natural Science Foundation of China (Nos. 82060386, 82272440, 52262014), the Hainan Provincial Natural Science Foundation of China (No. 823CXTD376), the CAMS Innovation Fund for Medical Sciences (No. 2019-I2M-5-023), and the Key Laboratory Open Project Fund of Emergency and Trauma of Ministry of Education (No. KLET-202008).

■ REFERENCES

(1) Cao, L.; Wang, P.; Chen, L.; Wu, Y.; Di, J. A photoelectrochemical glucose sensor based on gold nanoparticles as a mimic enzyme of glucose oxidase. *RSC Adv.* **2019**, *9*, 15307−15313.

(2) Wang, C.; Nie, X.-G.; Shi, Y.; Zhou, Y.; Xu, J.-J.; Xia, X.-H.; Chen, H.-Y. Direct plasmon-accelerated electrochemical reaction on gold nanoparticles. *ACS Nano* **2017**, *11*, 5897−5905.

(3) Chen, D.; Zou, X.; Dong, F.; Zhen, C.; Xiao, D.; Wang, X.; Wu, Q.; Cao, Y.; Tu, J. Donor-acceptor compensated ZnO semiconductor for photoelectrochemical biosensors. *ACS Appl. Mater. Interfaces* **2021**, *13*, 33006−33014.

(4) Cui, H.; Yao, C.; Cang, Y.; Liu, W.; Zhang, Z.; Miao, Y.; Xin, Y. Oxygen vacancy-regulated TiO_2 nanotube photoelectrochemical sensor for highly sensitive and selective detection of tetracycline hydrochloride. *Sens. Actuators, B* **2022**, *359*, No. 131564.

(5) Kang, J.; Zhang, Y.; Chai, Z.; Qiu, X.; Cao, X.; Zhang, P.; Teobaldi, G.; Liu, L.-M.; Guo, L. Amorphous domains in black titanium dioxide. *Adv. Mater.* **2021**, *33*, No. 2100407.

(6) Kumaravel, V.; Bartlett, J.; Pillai, S. C. Photoelectrochemical conversion of carbon dioxide (CO_2) into fuels and value-added products. *ACS Energy Lett.* **2020**, *5*, 486−519.

(7) Cai, G.; Yu, Z.; Ren, R.; Tang, D. Exciton−plasmon interaction between AuNPs/graphene nanohybrids and CdS quantum dots/TiO_2 for photoelectrochemical aptasensing of prostate-specific antigen. *ACS Sens.* **2018**, *3*, 632−639.

(8) Chen, Y.; Li, X.; Cai, G.; Li, M.; Tang, D. In situ formation of (001)TiO_2/Ti_3C_2 heterojunctions for enhanced photoelectrochemical detection of dopamine. *Electrochem. Commun.* **2021**, *125*, No. 106987.

(9) Qiu, Z.; Shu, J.; Tang, D. Near-infrared-to-ultraviolet light-mediated photoelectrochemical aptasensing platform for cancer biomarker based on core−shell NaYF4:Yb,Tm@TiO_2 upconversion microrods. *Anal. Chem.* **2018**, *90*, 1021−1028.

(10) Shu, J.; Qiu, Z.; Lv, S.; Zhang, K.; Tang, D. Plasmonic enhancement coupling with defect-engineered TiO_{2-x}: A mode for sensitive photoelectrochemical biosensing. *Anal. Chem.* **2018**, *90*, 2425−2429.

(11) Tayebi, M.; Kolaei, M.; Tayyebi, A.; Masoumi, Z.; Belbasi, Z.; Lee, B.-K. Reduced graphene oxide (RGO) on TiO_2 for an improved photoelectrochemical (PEC) and photocatalytic activity. *Sol. Energy* **2019**, *190*, 185−194.

(12) Chen, X.; Li, J.; Pan, G.; Xu, W.; Zhu, J.; Zhou, D.; Li, D.; Chen, C.; Lu, G.; Song, H. Ti_3C_2 mxene quantum dots/TiO_2 inverse opal heterojunction electrode platform for superior photoelectrochemical biosensing. *Sens. Actuators, B* **2019**, *289*, 131−137.

(13) Lv, S.; Li, Y.; Zhang, K.; Lin, Z.; Tang, D. Carbon dots/g-C_3N_4 nanoheterostructures-based signal-generation tags for photoelectrochemical immunoassay of cancer biomarkers coupling with copper nanoclusters. *ACS Appl. Mater. Interfaces* **2017**, *9*, 38336−38343.

(14) Lin, Y.; Zhou, Q.; Tang, D.; Niessner, R.; Knopp, D. Signal-on photoelectrochemical immunoassay for aflatoxin B1 based on enzymatic product-etching MnO_2 nanosheets for dissociation of carbon dots. *Anal. Chem.* **2017**, *89*, 5637−5645.

(15) Zhang, Y.; Xu, M.; Li, H.; Ge, H.; Bian, Z. The enhanced photoreduction of Cr(VI) to Cr(III) using carbon dots coupled TiO_2 mesocrystals. *Appl. Catal., B* **2018**, *226*, 213−219.

(16) Ke, J.; Li, X.; Zhao, Q.; Liu, B.; Liu, S.; Wang, S. Upconversion carbon quantum dots as visible light responsive component for efficient enhancement of photocatalytic performance. *J. Colloid Interface Sci.* **2017**, *496*, 425−433.
(17) Zhu, J.; Zhang, M.; Xiong, J.; Yan, Y.; Li, W.; Cheng, G. Electrostatically assembled construction of ternary TiO_2-Cu@C hybrid with enhanced solar-to-hydrogen evolution employing amorphous carbon dots as electronic mediator. *Chem. Eng. J.* **2019**, *375*, No. 121902.
(18) Wang, C.; Shi, Y.; Dan, Y.-Y.; Nie, X.-G.; Li, J.; Xia, X.-H. Enhanced peroxidase-like performance of gold nanoparticles by hot electrons. *Chem. - Eur. J.* **2017**, *23*, 6717−6723.
(19) Wang, Y.; Ge, S.; Zhang, L.; Yu, J.; Yan, M.; Huang, J. Visible photoelectrochemical sensing platform by in situ generated CdS quantum dots decorated branched-TiO_2 nanorods equipped with prussian blue electrochromic display. *Biosens. Bioelectron.* **2017**, *89*, 859−865.
(20) Li, X.; Sun, Z.; Bao, Y.; Xia, X.; Tao, T.; Homewood, K. P.; Li, R.; Gao, Y. Comprehensively improved hydrogen sensing performance via constructing the facets homojunction in rutile TiO_2 hierarchical structure. *Sens. Actuators, B* **2022**, *350*, No. 130869.
(21) Qu, S.; Wang, X.; Lu, Q.; Liu, X.; Wang, L. A biocompatible fluorescent ink based on water-soluble luminescent carbon nanodots. *Angew. Chem. Int. Ed.* **2012**, *51*, 12215−12218.
(22) Cao, M.; Li, Y.; Zhao, Y.; Shen, C.; Zhang, H.; Huang, Y. A novel method for the preparation of solvent-free, microwave-assisted and nitrogen-doped carbon dots as fluorescent probes for chromium(VI) detection and bioimaging. *RSC Adv.* **2019**, *9*, 8230−8238.
(23) Ran, X.; Qu, Q.; Qian, X.; Xie, W.; Li, S.; Li, L.; Yang, L. Water-soluble pillar[6]arene functionalized nitrogen-doped carbon quantum dots with excellent supramolecular recognition capability and superior electrochemical sensing performance towards TNT. *Sens. Actuators, B* **2018**, *257*, 362−371.
(24) Gao, C.; Wei, T.; Zhang, Y.; Song, X.; Huan, Y.; Liu, H.; Zhao, M.; Yu, J.; Chen, X. A photoresponsive rutile TiO_2 heterojunction with enhanced electron−hole separation for high-performance hydrogen evolution. *Adv. Mater.* **2019**, *31*, No. 1806596.
(25) Liao, X.; Xu, Q.; Sun, H.; Liu, W.; Chen, Y.; Xia, X.-H.; Wang, C. Plasmonic nanozymes: Localized surface plasmonic resonance regulates reaction kinetics and antibacterial performance. *J. Phys. Chem. Lett.* **2022**, *13*, 312−323.
(26) Lee, S.; Cho, I.-S.; Lee, J. H.; Kim, D. H.; Kim, D. W.; Kim, J. Y.; Shin, H.; Lee, J.-K.; Jung, H. S.; Park, N.-G.; Kim, K.; Ko, M. J.; Hong, K. S. Two-step sol-gel method-based TiO_2 nanoparticles with uniform morphology and size for efficient photo-energy conversion devices. *Chem. Mater.* **2010**, *22*, 1958−1965.
(27) Wang, T.; Li, W.; Xu, D.; Wu, X.; Cao, L.; Meng, J. A novel and facile synthesis of black TiO_2 with improved visible-light photocatalytic H_2 generation: Impact of surface modification with ctab on morphology, structure and property. *Appl. Surf. Sci.* **2017**, *426*, 325−332.
(28) Wang, F.; Wu, Y.; Wang, Y.; Li, J.; Jin, X.; Zhang, Q.; Li, R.; Yan, S.; Liu, H.; Feng, Y.; Liu, G.; Lv, W. Construction of novel z-scheme nitrogen-doped carbon dots/{001} TiO_2 nanosheet photocatalysts for broad-spectrum-driven diclofenac degradation: Mechanism insight, products and effects of natural water matrices. *Chem. Eng. J.* **2019**, *356*, 857−868.
(29) Yu, S.; Zhong, Y.-Q.; Yu, B.-Q.; Cai, S.-Y.; Wu, L.-Z.; Zhou, Y. Graphene quantum dots to enhance the photocatalytic hydrogen evolution efficiency of anatase TiO_2 with exposed {001} facet. *Phys. Chem. Chem. Phys.* **2016**, *18*, 20338−20344.
(30) Ou, N.-Q.; Li, H.-J.; Lyu, B.-W.; Gui, B.-J.; Sun, X.; Qian, D.-J.; Jia, Y.; Wang, X.; Yang, J. Facet-dependent interfacial charge transfer in TiO_2/nitrogen-doped graphene quantum dots heterojunctions for visible-light driven photocatalysis. *Catalysts* 2019, *9*, DOI: 10.3390/catal9040345.
(31) Rajender, G.; Kumar, J.; Giri, P. K. Interfacial charge transfer in oxygen deficient TiO_2-graphene quantum dot hybrid and its influence on the enhanced visible light photocatalysis. *Appl. Catal., B* **2018**, *224*, 960−972.
(32) Zhou, T.; Chen, S.; Li, L.; Wang, J.; Zhang, Y.; Li, J.; Bai, J.; Xia, L.; Xu, Q.; Rahim, M.; Zhou, B. Carbon quantum dots modified anatase/rutile TiO_2 photoanode with dramatically enhanced photoelectrochemical performance. *Appl. Catal., B* **2020**, *269*, No. 118776.
(33) Ye, K.-H.; Wang, Z.; Gu, J.; Xiao, S.; Yuan, Y.; Zhu, Y.; Zhang, Y.; Mai, W.; Yang, S. Carbon quantum dots as a visible light sensitizer to significantly increase the solar water splitting performance of bismuth vanadate photoanodes. *Energy Environ. Sci.* **2017**, *10*, 772−779.
(34) Hui, K. C.; Ang, W. L.; Yahya, W. Z. N.; Sambudi, N. S. Effects of nitrogen/bismuth-doping on the photocatalyst composite of carbon dots/titanium dioxide nanoparticles (CDs/TNP) for enhanced visible light-driven removal of diclofenac. *Chemosphere* **2022**, *290*, No. 133377.
(35) Liao, X.; Zhao, X.; Tan, Z.; Wang, C.; Liu, W. Au nanoparticles in 2D bimetallic metal−organic frameworks with enhanced plasmonic nanozyme activity for antibacterial therapy. *ACS Appl. Nano Mater.* **2022**, *5*, 16145−16153.
(36) Kang, J.; Qiu, X.; Hu, Q.; Zhong, J.; Gao, X.; Huang, R.; Wan, C.; Liu, L.-M.; Duan, X.; Guo, L. Valence oscillation and dynamic active sites in monolayer NiCo hydroxides for water oxidation. *Nat. Catal.* **2021**, *4*, 1050−1058.
(37) Tian, L.; Li, Z.; Wang, P.; Zhai, X. H.; Wang, X.; Li, T. X. Carbon quantum dots for advanced electrocatalysis. *J. Energy Chem.* **2021**, *55*, 279−294.
(38) Gao, Y.; Zeng, Y.; Liu, X.; Tang, D. Liposome-mediated in situ formation of type-I heterojunction for amplified photoelectrochemical immunoassay. *Anal. Chem.* **2022**, *94*, 4859−4865.
(39) Zeng, R.; Xu, J.; Liang, T.; Li, M.; Tang, D. Photocurrent-polarity-switching photoelectrochemical biosensor for switching spatial distance electroactive tags. *ACS Sens.* **2023**, *8*, 317−325.
(40) Xu, L.; Xia, J.; Wang, L.; Qian, J.; Li, H.; Wang, K.; Sun, K.; He, M. Alpha-Fe_2O_3 cubes with high visible-light-activated photoelectrochemical activity towards glucose: Hydrothermal synthesis assisted by a hydrophobic ionic liquid. *Chem. - Eur. J.* **2014**, *20*, 2244−2253.
(41) Wang, W.; Bao, L.; Lei, J.; Tu, W.; Ju, H. Visible light induced photoelectrochemical biosensing based on oxygen-sensitive quantum dots. *Anal. Chim. Acta* **2012**, *744*, 33−38.
(42) Zhang, X.; Liu, M.; Liu, H.; Zhang, S. Low-toxic Ag_2S quantum dots for photoelectrochemical detection glucose and cancer cells. *Biosens. Bioelectron.* **2014**, *56*, 307−312.
(43) Devadoss, A.; Sudhagar, P.; Das, S.; Lee, S. Y.; Terashima, C.; Nakata, K.; Fujishima, A.; Choi, W. B.; Kang, Y. S.; Paik, U. Synergistic metal-metal oxide nanoparticles supported electrocatalytic graphene for improved photoelectrochemical glucose oxidation. *ACS Appl. Mater. Interfaces* **2014**, *6*, 4864−4871.
(44) Du, J.; Yu, X.; Wu, Y.; Di, J. ZnS nanoparticles electrodeposited onto ITO electrode as a platform for fabrication of enzyme-based biosensors of glucose. *Mater. Sci. Eng., C* **2013**, *33*, 2031−2036.
(45) Xia, L.; Song, J.; Xu, R.; Liu, D.; Dong, B.; Xu, L.; Song, H. Zinc oxide inverse opal electrodes modified by glucose oxidase for electrochemical and photoelectrochemical biosensor. *Biosens. Bioelectron.* **2014**, *59*, 350−357.
(46) Liu, X.; Huo, X.; Liu, P.; Tang, Y.; Xu, J.; Liu, X.; Zhou, Y. Assembly of MoS_2 nanosheet-TiO_2 nanorod heterostructure as sensor scaffold for photoelectrochemical biosensing. *Electrochim. Acta* **2017**, *242*, 327−336.
(47) Zheng, M.; Cui, Y.; Li, X.; Liu, S.; Tang, Z. Photoelectrochemical sensing of glucose based on quantum dot and enzyme nanocomposites. *J. Electroanal. Chem.* **2011**, *656*, 167−173.

https://doi.org/10.1021/acsomega.3c02202
ACS Omega 2023, 8, 22099−22107